

Imaging Stacking Order in Few-Layer Graphene

Chun Hung Lui,[†] Zhiqiang Li,[†] Zheyuan Chen,[†] Paul V. Klimov,^{†,§} Louis E. Brus,[†] and Tony F. Heinz^{*,†}

[†]Departments of Physics and Electrical Engineering, Columbia University, 538 West 120th Street, New York, New York 10027, United States, and [‡]Department of Chemistry, Columbia University, 3000 Broadway, New York, New York 10027, United States

ABSTRACT Few-layer graphene (FLG) has been predicted to exist in various crystallographic stacking sequences, which can strongly influence the material's electronic properties. We demonstrate an accurate and efficient method to characterize stacking order in FLG using the distinctive features of the Raman 2D-mode. Raman imaging allows us to visualize directly the spatial distribution of Bernal (ABA) and rhombohedral (ABC) stacking in tri- and tetralayer graphene. We find that 15% of exfoliated graphene tri- and tetralayers is composed of micrometer-sized domains of rhombohedral stacking, rather than of usual Bernal stacking. These domains are stable and remain unchanged for temperatures exceeding 800 °C.

KEYWORDS Graphene, trilayer, few layer, stacking order, Raman

Graphene-based materials have stimulated intense interest because of their remarkable electronic properties and potential for novel applications. With the impressive progress in research on graphene mono- and bilayers, recent attention has also turned to graphene's few-layer counterparts.^{1–7} In few-layer graphene (FLG), the crystallographic stacking of the individual graphene sheets provides an additional degree of freedom.^{4,8–11} The distinct lattice symmetries associated with different stacking orders of FLG have been predicted to strongly influence the electronic properties of FLG,^{3,4,8–23} including the band structure,^{8,10,12–19} interlayer screening,²⁰ magnetic state,^{22,23} and spin–orbit coupling.²¹ Experimentally, the strong influence of stacking order on the low-energy electronic structure of FLG was recently demonstrated by infrared (IR) spectroscopy.⁴ For graphene trilayers, two stable crystallographic configurations are predicted: ABA and ABC stacking order^{8–10,12,13} (Figure 1). In the absence of direct evidence of ABC stacking order in trilayers, ABA stacking order has generally been presumed in most studies of exfoliated materials, as this structure is believed to be slightly more thermodynamically stable than the ABC stacking order. Recent studies,^{3,8–10,12,14,16,17,19,20,24} however, indicate distinct properties for these two types of graphene trilayers. ABA-stacked trilayers are semimetals with an electrically tunable band overlap,^{3,10,12,16–18} while ABC-stacked trilayers are predicted to be semiconductors with an electrically tunable band gap.^{10,12,15,19} In view of these differences, research on

FLG requires the development of convenient and accurate methods for characterizing stacking order and its spatial distribution.

While IR spectroscopy provides a means of identifying stacking order in FLG,⁴ it requires somewhat specialized instrumentation and cannot provide high spatial resolution. Raman spectroscopy, on the other hand, has the potential to overcome these limitations and serves as an effective general approach for characterization and spatial imaging of stacking order. The technique has already proved to be a reliable and efficient method for determining many physical properties of graphene layers.^{6,25} The intensity of the D-mode indicates the defect density,²⁵ the peak position and line shape of the G-mode reflect the doping^{25,26} and strain level.^{27,28} In addition, the 2D (G') mode, arising from a double-resonant electronic process,^{6,25,29,30} is sensitive not only to the vibrational features of graphene, but also to its electronic structure. As such, its line shape provides an accurate signature of graphene mono- and bilayers.^{6,25,31,32}

In this Letter, we demonstrate that stacking order in tri- and tetralayer graphene samples can be readily identified by means of Raman spectroscopy. We find that both Bernal (ABA) and rhombohedral (ABC) stacking order are present in exfoliated samples, and the different structures are associated with distinctive line shapes in the Raman 2D mode. The rhombohedral samples show a more asymmetric 2D feature with an enhanced peak and shoulder, compared with the feature seen in Bernal samples. Taking advantage of this difference in line shape, we were able to visualize stacking domains in exfoliated tri- and tetralayer graphene with micrometer spatial resolution. Even in samples of completely homogeneous layer thickness, we observed domains of different stacking order, with approximately 15% of the total area displaying rhombohedral stacking.

* To whom correspondence should be addressed. E-mail: tony.heinz@columbia.edu.

[§] Current address: Center for Spintronics and Quantum Computation, University of California, Santa Barbara, California 93106, USA.

Received for review: 09/16/2010

Published on Web: 12/01/2010

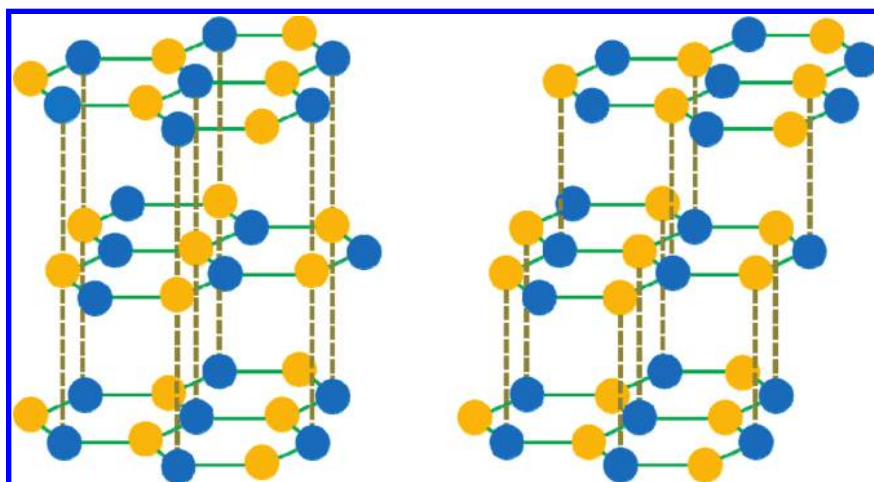


FIGURE 1. Lattice structure of trilayer graphene with ABA (left) and ABC (right) stacking sequence. The yellow and blue dots represent carbon atoms in the A and B sublattices of the graphene honeycomb structure.

In our experiment, we prepared FLG samples by mechanical exfoliation of kish graphite (Toshiba) on both bulk SiO₂ (Chemglass, Inc.) and Si substrates covered with a 300-nm-thick oxide layer. The substrates were cleaned by etching in piranha (sulfuric acid and hydrogen peroxide) solution. The typical area of our graphene samples varied from several hundreds to thousands of square micrometers. We first examined the samples by IR spectroscopy. This technique permits accurate determination of layer thickness in FLG and, through the differences in the low-energy electronic structure, also of the stacking order.⁴ We observed two distinct groups of IR spectra both for the trilayer and tetralayer graphene, corresponding to Bernal (ABA) and rhombohedral (ABC) stacking (see Supporting Information and ref 4 for details). We then performed Raman measurement on the same FLG samples. Raman spectra were collected in a backscattering geometry using linearly polarized laser radiation at wavelengths (photon energies) of 633 nm (1.96 eV), 597 nm (2.09 eV), 514 nm (2.41 eV), and 458 nm (2.71 eV). The laser beam was focused to a spot size of $\sim 1 \mu\text{m}$ on the graphene samples. We obtained Raman spatial maps for an excitation wavelength of 514 nm by raster scanning with a precision two-dimensional stage having a step size of 0.5 or 1 μm .³³ For such spatial mapping of the Raman response, we generally used a spectral resolution of $\sim 8 \text{ cm}^{-1}$ (obtained with a 600 grooves/mm grating). For the measurement of key spectra, however, a spectral resolution of $\sim 2 \text{ cm}^{-1}$ (1800 grooves/mm grating) was chosen to elucidate the details of the line shape.

We observed consistent differences in the line shape of the Raman 2D-mode between samples with Bernal and rhombohedral stacking. Figure 2 displays results for trilayer samples. For all excitation photon energies, the ABC trilayers displayed more asymmetric and broader lines than ABA trilayers. In particular, we observed a sharp peak and an enhanced shoulder in the ABC spectra for all excitation photon energies. (More detailed analysis of the spectra can

be found in the Supporting Information.) This signature of stacking order is clear in all pristine trilayer samples. (We note that chemically processed samples may exhibit broadened 2D-mode spectra from doping and disorder. This may obscure the stacking-order signature.)

While the 2D mode has been applied widely to identify mono- and bilayer samples,^{6,25,31,32} its application to analysis of trilayers has been more limited because of the lack of consensus on the 2D line shape of different trilayer samples. This mode was found to have a more asymmetric shape in some studies^{6,34,35} and a less asymmetric shape in others.³² Our results suggest that such variation may arise from the difference in stacking order among samples.

We have also examined the Raman G-mode of ABA and ABC trilayer graphene (Figure 3). The spectra were taken in ABA and ABC stacking domains of a single trilayer sample to maintain similar doping and strain conditions. (Detailed information about the coexistence of such stacking domains is discussed below.) Only slight differences are observable in the G-mode frequency and line shape, as well as in the 2D/G ratio. As the G-mode is not influenced by electronic resonances, we ascribe the small red shift ($\sim 1 \text{ cm}^{-1}$) of the G-mode frequency of the ABC trilayer compared to the ABA trilayer to the slight difference of their phonon band structures.³⁶ In addition, the very weak D-mode feature [D/G < 0.005, as shown in the inset of Figure 3b] indicates the high crystalline quality in the trilayer areas of either stacking order.

The similarity of the G-mode features in ABA and ABC trilayers implies that the greater sensitivity of the 2D mode to stacking order is the result of differences in electronic structure. The Raman 2D mode is expected to be affected by the electronic properties since it arises from a double-resonance process that involves transitions among various electronic states.^{6,25,29,30} It is this sensitivity that has rendered the 2D-mode a fingerprint for mono- and bilayer graphene samples.^{25,31}

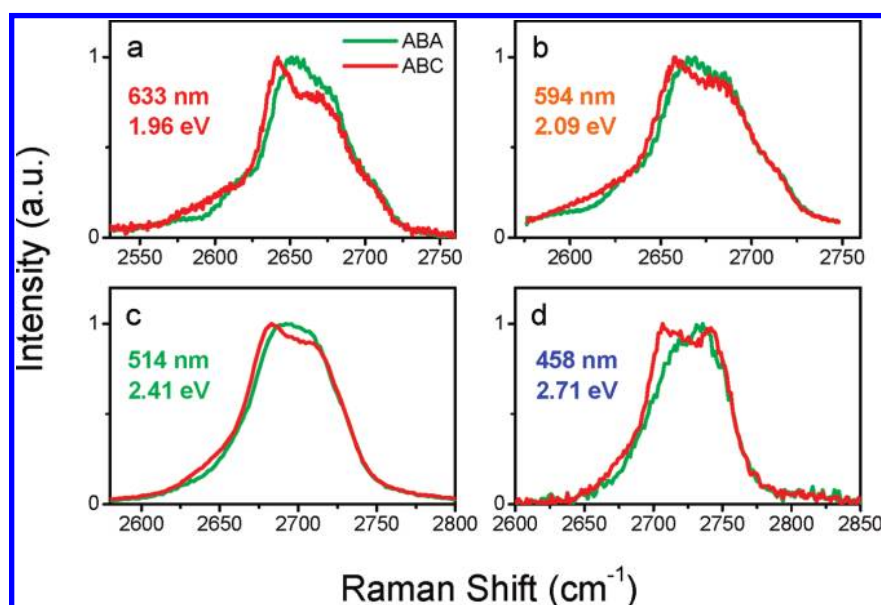


FIGURE 2. Raman spectra of the 2D-mode of ABA (green line) and ABC (red line) trilayer graphene samples at four different laser excitation wavelengths. The increase in the average Raman shift with excitation photon energy is an expected consequence of the double-resonance process that selectively couples phonons with different momenta around the K -point.

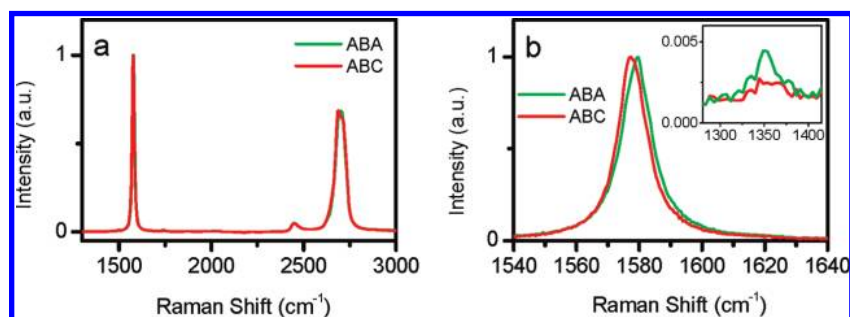


FIGURE 3. Raman spectra of graphene trilayers with ABA (green line) and ABC (red line) stacking order. (a) Raman spectra over a broad energy range. (b) Details of G-mode and D-mode (inset) spectra. The excitation laser wavelength is 514 nm.

In order to visualize the spatial distribution of the stacking domains, we implemented a method for Raman mapping. To this end, we needed to define a quantity that could effectively encode the differences between the Raman spectra for the two different stacking orders. We examined several schemes, including ones based on changes in the centroid and asymmetry of the Raman spectrum. We found, however, that using the spectral width of the 2D mode captured the differences in a simple and robust fashion. To extract the width, we fit the spectrum at each pixel in the spatial mapping to a single Lorentzian function. We then produced spatial images by displaying the full width at half-maximum (fwhm) of the fit function for each pixel in the image. A direct determination of the width from the spectra can also be used to generate spatial maps. This procedure led, however, to noisier images.

Figure 4 presents examples of Raman mapping of the trilayer graphene samples that exhibit domains of differing stacking order. For comparison, we also show optical images of these samples. No difference in the optical contrast is

observed across the full area of the samples, indicating that each sample is entirely homogeneous in thickness. We have further performed IR measurements to confirm the results of the Raman mapping. The IR spectra obtained in the different regions of these four samples corresponds precisely to those of ABA and ABC trilayers (Figure S1 in the Supporting Information).

We note that exfoliated graphene samples exhibit spatially inhomogeneous carrier doping effects when deposited on typical insulating substrates.^{35,37} Could this charging effect influence our Raman data? To address this issue, we investigated a trilayer sample with ABC stacking that was suspended over a quartz trench and, hence, isolated from any substrate effects. There was no observable change in the Raman 2D line shape between the free-standing sample that has negligible doping and samples supported on the quartz substrates that have estimated unintentional doping of $n \sim 5 \times 10^{12} \text{ cm}^{-2}$ (see Supporting Information). We therefore conclude that the line shape of the 2D-mode is not sensitive to a variation of doping density on the order of 10^{12} cm^{-2} .

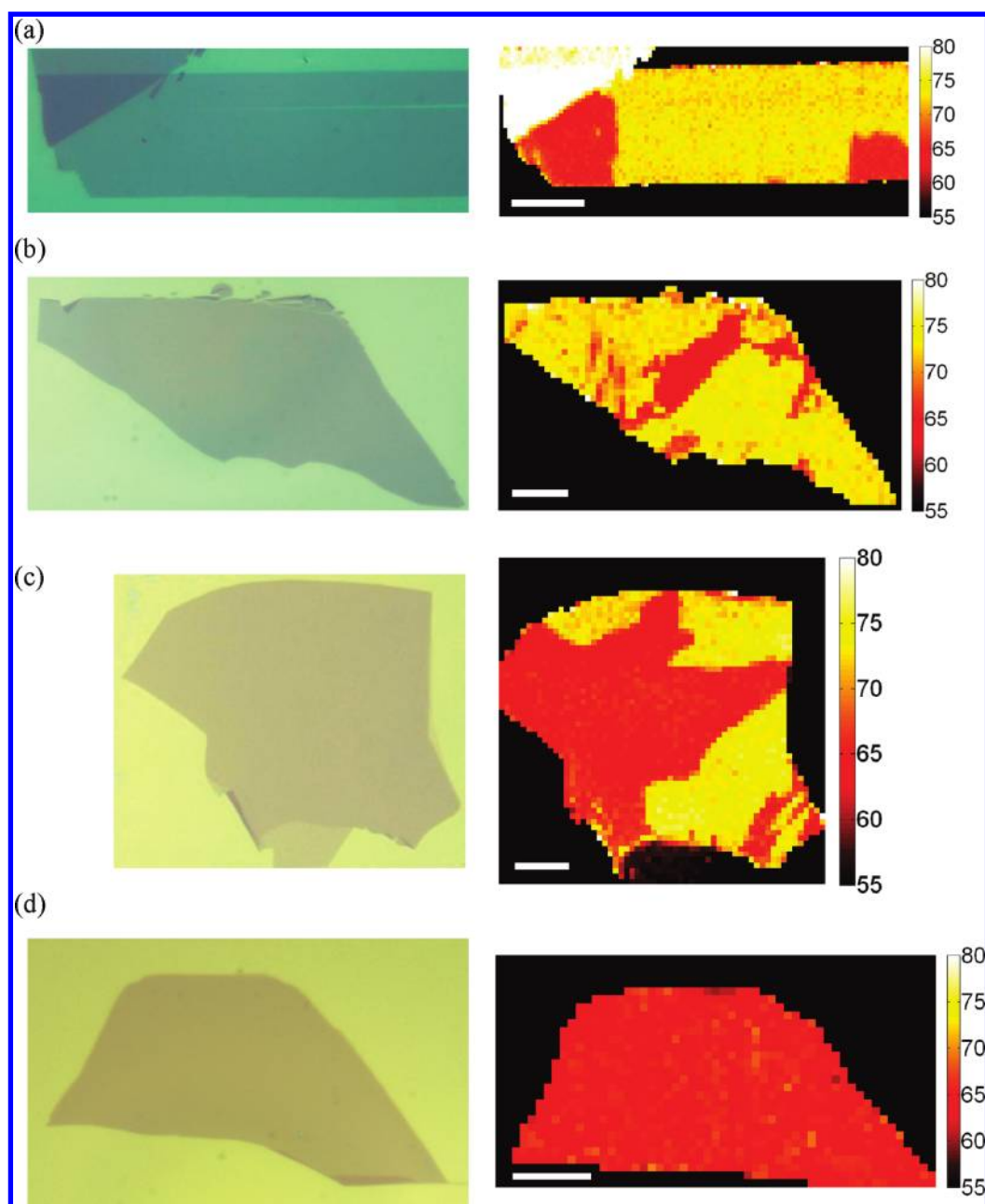


FIGURE 4. Optical images (left column) and spatial maps of the spectral width of the Raman 2D-mode feature (right column) for trilayer graphene samples. The homogeneity of the optical images shows the uniformity of the layer thickness of the four samples. The Raman images, taken with 514-nm excitation, are color coded according to the width of the Raman feature (fwhm in units of cm^{-1}). The red and yellow regions in the images correspond, respectively, to ABA and ABC trilayer graphene domains. The step size in the scans is $0.5 \mu\text{m}$ (a), and $1 \mu\text{m}$ (b–d). The scale bars are $10 \mu\text{m}$ in length. Similar results can be obtained using other wavelengths for the excitation laser.

The coexistence of ABA and ABC stacking order is striking. Among the 45 trilayer samples that we prepared, 26 exhibited purely ABA stacking, while 19 displayed mixed ABA and ABC stacking. None of the samples showed purely ABC stacking. In the 19 samples of mixed stacking order, only 5 samples contain large ($>200 \mu\text{m}^2$), homogeneous regions of ABC-stacking order, as in Figure 4a,c. If we consider the total area associated with the two different stacking orders, we find that $\sim 85\%$ of the area in our samples corresponds to ABA stacking, and $\sim 15\%$ cor-

responds to ABC stacking. This result is comparable to that obtained in earlier X-ray diffraction studies of graphite,^{58,59} which indicate that graphite typically contains 80% of the Bernal structure, 14% of the rhombohedral structure, and 6% of a disordered structure.⁵⁸ The similarity of our results suggests that the different stacking orders observed in trilayer graphene originate from the pristine structure of the graphite used in the exfoliation process, which is not modified during the exfoliation of the layers. This claim is supported by the complicated patterns of stacking domains in

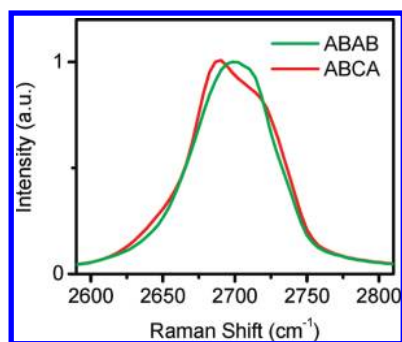


FIGURE 5. Raman 2D-mode spectra for the tetralayer graphene samples of ABAB (green line) and ABCA (red line) stacking order.

our samples. One would not expect these patterns to be produced by mechanical processing.

The method of imaging stacking order by Raman spectroscopy can be generalized to investigations of FLG of greater thickness. Here we show the results for tetralayer graphene. Figure 5 shows the 2D-mode Raman spectra for ABAB (green line) and ABCA (red line) tetralayer graphene (Detailed information on the stability and IR spectroscopy of these two types of tetralayer graphene can be found in refs 4 and 10). By carefully examining the spectra, we observed distinct line shapes for the two stacking orders. ABCA tetralayers show more structured, asymmetric lines with greater widths than the ABAB tetralayers. In particular, we observed a sharp peak and an enhanced shoulder in the ABCA spectrum at 2680 cm^{-1} and 2640 cm^{-1} . Such distinctions in the 2D-mode spectra are observed in all ABAB and ABCA tetralayer samples. We note that both the ABC trilayer (Figure 2c) and the ABCA tetralayer exhibit similar 2D-mode line shapes, indicating that the asymmetric and broadened features are characteristics of this stacking order.

Figure 6a,b shows, respectively, the optical image and Raman image of a tetralayer graphene sample with mixed (ABAB and ABCA) stacking order. The homogeneous optical image indicates that the sample is entirely graphene of four

layers in thickness. The Raman image, which encodes the 2D-mode spectral width (fwhm) extracted from a single Lorentzian fit, shows sharp contrast for regions of different stacking order. The stacking sequences determined by Raman spectroscopy in these domains were further confirmed by IR spectroscopy.

The characteristics of the stacking domains based on an analysis of 56 samples were found to be similar to those for trilayer graphene. In particular, the ratio of the area of ABAB to ABCA stacking was 85:15. The similarity of the domains in tetralayer and trilayer graphene confirms the common origin of the different stacking sequences, namely, the stacking order of the kish graphite, which remains unchanged during the exfoliation process.

The ability to directly visualize the domains of stacking order provides a means of assessing the thermodynamic stability of the different structures. Our Raman images show that Bernal and rhombohedral stacking order can coexist in micrometer-sized domains of trilayer thickness at room temperature. By annealing the samples in an argon environment, we found, by both Raman and IR spectroscopy, that the domains of rhombohedral stacking order are stable up to $800\text{ }^{\circ}\text{C}$, the maximum annealing temperature in our experiment. This result is consistent with the stability of bulk rhombohedral graphite to over $1000\text{ }^{\circ}\text{C}$.^{40,41} Our result shows that this stability is retained even for *atomically thin* rhombohedrally stacked crystallites (More detailed information on the annealing measurements can be found in the Supporting Information).

In conclusion, we have demonstrated Raman spectroscopy to be an effective tool for the characterization of stacking order in FLG. Bernal (ABA) and rhombohedral (ABC) tri- and tetralayer graphene samples exhibit clear differences in the line shape and width of the Raman 2D line. By Raman spatial mapping, we find that, for typical exfoliated tri- and tetralayer samples, about 15% of the area has rhombohedral stacking rather than the usual Bernal stacking. The domains

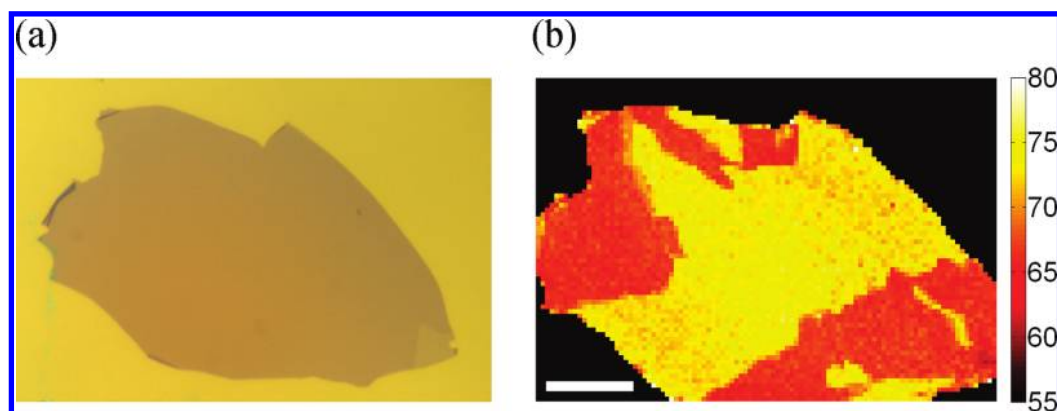


FIGURE 6. (a) Optical and (b) Raman images of a specific tetralayer graphene sample. The optical image shows the uniformity of the layer thickness of the sample. The Raman map of the spectral width of Raman 2D-mode exhibits domains with different stacking order. The Raman images, obtained with 514-nm excitation, are color coded according to the fwhm of the Raman feature (in units of cm^{-1}). The red and yellow regions in the images correspond, respectively, to tetralayer graphene with ABAB and ABCA stacking. The step size for the Raman mapping was $1\text{ }\mu\text{m}$. The length of the scale bar is $20\text{ }\mu\text{m}$.

of rhombohedral stacking are generally only of micrometer length. The Raman technique presented in this paper should accelerate the research on FLG. For instance, various studies^{10,12,15,19} have predicted that a significant and electrically tunable band gap can be opened in rhombohedral trilayer graphene by the application of an electric field. However, for Bernal trilayers with their differing symmetry, this effect will be much smaller. With the Raman technique presented here, we can readily identify the domains of stacking in FLG and can test these predictions experimentally by constructing an appropriate gated device. In addition to assuring the desired crystal structure of samples, the Raman mapping capabilities allow identification of domain boundaries. This information should permit detailed exploration of the structural and electronic properties at these interfaces.

Acknowledgment. We thank K. F. Mak, L. M. Malard, S. Ryu, and J. Shan for discussions. We acknowledge support from the Office of Naval Research under the MURI program, from DOE Basic Energy Sciences under grants DE-FG02-98ER14861 and DE-FG02-07ER15842, from the National Science Foundation under Grant CHE-0117752 and the NRI program of the SRC, and from the New York State Office of Science, Technology, and Academic Research (NYSTAR).

Supporting Information Available. The material contains the results of the IR spectroscopy, detailed analysis of the Raman spectra of ABA and ABC graphene trilayers, information of the influence of the substrate on the 2D-mode line shape, and additional discussion about the thermal stability of ABC stacking order. This material is available free of charge via the Internet at <http://pubs.acs.org>.

REFERENCES AND NOTES

- Ohta, T.; Bostwick, A.; McChesney, J. L.; Seyller, T.; Horn, K.; Rotenberg, E. *Phys. Rev. Lett.* **2007**, *98*, 206802.
- Mak, K. F.; Sfeir, M. Y.; Misewich, J. A.; Heinz, T. F. *Proc. Natl. Acad. Sci. U.S.A.* **2010**, *107*, 14999.
- Craciun, M. F.; Russo, S.; Yamamoto, M.; Oostinga, J. B.; Morpurgo, A. F.; Thruha, S. *Nat. Nanotechnol.* **2009**, *4*, 383.
- Mak, K. F.; Shan, J.; Heinz, T. F. *Phys. Rev. Lett.* **2010**, *104*, 176404.
- Bruna, M.; Borini, S. *Phys. Rev. B* **2010**, *81*, 125421.
- Malard, L. M.; Pimenta, M. A.; Dresselhaus, G.; Dresselhaus, M. S. *Phys. Rep.* **2009**, *473*, 51.
- Jung, N.; Kim, N.; Jockusch, S.; Turro, N. J.; Kim, P.; Brus, L. *Nano Lett.* **2009**, *9*, 4133.
- Latil, S.; Henrard, L. *Phys. Rev. Lett.* **2006**, *97*, No. 036803.
- Min, H. K.; MacDonald, A. H. *Prog. Theor. Phys. Suppl.* **2008**, *176*, 227.
- Aoki, M.; Amawashi, H. *Solid State Commun.* **2007**, *142*, 123.
- Norimatsu, W.; Kusunoki, M. *Phys. Rev. B* **2010**, *81*, 161410.
- Guinea, F.; Neto, A. H. C.; Peres, N. M. R. *Phys. Rev. B* **2006**, *73*, 245426.
- Guinea, F.; Castro, A. H.; Peres, N. M. R. *Solid State Commun.* **2007**, *143*, 116.
- Lu, C. L.; Chang, C. P.; Huang, Y. C.; Ho, J. H.; Hwang, C. C.; Lin, M. F. *J. Phys. Soc. Jpn.* **2007**, *76*, No. 024701.
- Chang, C. P.; Wang, J.; Lu, C. L.; Huang, Y. C.; Lin, M. F.; Chen, R. B. *J. Appl. Phys.* **2008**, *103*, 103109.
- Avetisyan, A. A.; Partoens, B.; Peeters, F. M. *Phys. Rev. B* **2009**, *80*, 195401.
- Avetisyan, A. A.; Partoens, B.; Peeters, F. M. *Phys. Rev. B* **2009**, *79*, No. 035421.
- Koshino, M.; McCann, E. *Phys. Rev. B* **2009**, *79*, 125443.
- Avetisyan, A. A.; Partoens, B.; Peeters, F. M. *Phys. Rev. B* **2010**, *81*, 115432.
- Koshino, M. *Phys. Rev. B* **2010**, *81*, 125304.
- McCann, E.; Koshino, M. *Phys. Rev. B* **2010**, *81*, 241409.
- Otani, M.; Koshino, M.; Takagi, Y.; Okada, S. *Phys. Rev. B* **2010**, *81*, 161403.
- Otani, M.; Takagi, Y.; Koshino, M.; Okada, S. *Appl. Phys. Lett.* **2010**, *96*, 242504.
- Nakamura, M.; Hirasawa, L. *Phys. Rev. B* **2008**, *77*, No. 045429.
- Ferrari, A. C. *Solid State Commun.* **2007**, *143*, 47.
- Das, A.; Pisana, S.; Chakraborty, B.; Piscanec, S.; Saha, S. K.; Waghmare, U. V.; Novoselov, K. S.; Krishnamurthy, H. R.; Geim, A. K.; Ferrari, A. C.; Sood, A. K. *Nat. Nanotechnol.* **2008**, *3*, 210.
- Huang, M. Y.; Yan, H. G.; Chen, C. Y.; Song, D. H.; Heinz, T. F.; Hone, J. *Proc. Natl. Acad. Sci. U.S.A.* **2009**, *106*, 7304.
- Mohiuddin, T. M. G.; Lombardo, A.; Nair, R. R.; Bonetti, A.; Savini, G.; Jalil, R.; Bonini, N.; Basko, D. M.; Galotis, C.; Marzari, N.; Novoselov, K. S.; Geim, A. K.; Ferrari, A. C. *Phys. Rev. B* **2009**, *79*, 205433.
- Thomsen, C.; Reich, S. *Phys. Rev. Lett.* **2000**, *85*, 5214.
- Saito, R.; Jorio, A.; Souza Filho, A. G.; Dresselhaus, G.; Dresselhaus, M. S.; Pimenta, M. A. *Phys. Rev. Lett.* **2001**, *88*, No. 027401.
- Ferrari, A. C.; Meyer, J. C.; Scardaci, V.; Casiraghi, C.; Lazzeri, M.; Mauri, F.; Piscanec, S.; Jiang, D.; Novoselov, K. S.; Roth, S.; Geim, A. K. *Phys. Rev. Lett.* **2006**, *97*, 187401.
- Park, J. S.; Reina, A.; Saito, R.; Kong, J.; Dresselhaus, G.; Dresselhaus, M. S. *Carbon* **2009**, *47*, 1303.
- Berciaud, S.; Ryu, S.; Brus, L. E.; Heinz, T. F. *Nano Lett.* **2009**, *9*, 346.
- Malard, L. M.; Guimaraes, M. H. D.; Mafra, D. L.; Mazzoni, M. S. C.; Jorio, A. *Phys. Rev. B* **2009**, *79*, 125426.
- Graf, D.; Molitor, F.; Ensslin, K.; Stampfer, C.; Jungen, A.; Hierold, C.; Wirtz, L. *Nano Lett.* **2007**, *7*, 238.
- Yan, J. A.; Ruan, W. Y.; Chou, M. Y. *Phys. Rev. B* **2008**, *77*, 125401.
- Stampfer, C.; Molitor, F.; Graf, D.; Ensslin, K.; Jungen, A.; Hierold, C.; Wirtz, L. *Appl. Phys. Lett.* **2007**, *91*, 241907.
- Lipson, H.; Stokes, A. R. *Proc. R. Soc. A* **1942**, *181*, No. 101.
- Wilhelm, H. A.; Croset, B.; Medjahdi, G. *Carbon* **2007**, *45*, 2356.
- Matuyama, E. *Nature* **1956**, *178*, 1459.
- Freise, E. J.; Kelly, A. *Philos. Mag.* **1963**, *8*, 1519.